VETOR

# Parameter Estimation and Strain Energy Model Class Selection for a Hyperelastic Composite Under Compression☆

## Estimativa de Parâmetros e Seleção de Classe de Modelos de Energia de Deformação em um Compósito Hiperelástico Submetido a Compressão

Lucas da Silva Asth[1†], Kauê Calenzani de Lima[1], Carolina Seixas Moreira[2], Diego Campos Knupp[1], Leonardo Tavares Stutz[1]

[1]*Instituto Politécnico, Universidade do Estado do Rio de Janeiro, Nova Friburgo, Brasil*
[2]*Departamento de Engenharia Mecânica, Faculdade de Engenharia, Universidade do Estado do Rio de Janeiro, Rio de Janeiro, Brasil*
[†]**Corresponding author:** lucas.asth@iprj.uerj.br

**Abstract**

The study of the mechanical behavior of human muscle tissues has received increasing attention due to its relevance in biomechanical and biomedical applications, and is often described by hyperelastic models because of its nonlinear response under mechanical loading. In this context, constitutive modeling requires the definition of an appropriate strain energy density function; however, there is still no universal model capable of satisfactorily representing all classes of soft hyperelastic materials, which makes the use of systematic methodologies for parameter identification and model selection essential. Thus, the present work aims to apply a Bayesian inverse problem approach, through the Transitional Markov Chain Monte Carlo (TMCMC) method, to determine, based on experimental data from uniaxial compression tests carried out on a pure hyperelastic material and on a hyperelastic composite reinforced with unidirectional fibers, which strain energy density models best represent the observed response. The TMCMC method stands out for providing a robust and efficient exploration of posterior distributions, allowing not only the estimation of constitutive parameters, but also the quantification of the uncertainties associated with these parameters and the probabilistic comparison among competing models through Bayesian evidence. The results highlight the importance of using methods that explicitly incorporate experimental and inferential uncertainties, since different models may present similar fits under an exclusively deterministic analysis.

**Keywords**

Hyperelastic materials • Strain energy model • Inverse problem • Transitional Markov Chain Monte Carlo (TMCMC)

**Resumo**

O estudo do comportamento mecânico de tecidos musculares humanos tem recebido crescente atenção devido à sua relevância em aplicações biomecânicas e biomédicas, sendo frequentemente descrito por modelos hiperelásticos em razão de sua resposta não linear sob carregamentos mecânicos. Nesse contexto, a modelagem constitutiva requer a definição de uma função de energia de deformação apropriada; entretanto, ainda não existe um modelo universal capaz de representar satisfatoriamente todas as classes de materiais hiperelásticos macios, o que torna fundamental o uso de metodologias sistemáticas para identificação paramétrica e seleção de modelos. Assim, este trabalho tem

☆This article is an extended version of the work presented at the XXVIII National Meeting on Computational Modeling (ENMC) & XVI Meeting on Science and Technology of Materials (ECTM), held in Montes Claros, Brazil, October 21–24, 2025.

como objetivo aplicar uma abordagem Bayesiana de solução de problemas inversos, por meio do método Transitional Markov Chain Monte Carlo (TMCMC), para determinar, com base em dados experimentais de ensaios de compressão uniaxial realizados em um material hiperelástico puro e em um compósito hiperelástico reforçado por fibras unidirecionais, quais modelos de energia de deformação melhor representam a resposta observada. O método TMCMC destaca-se por promover uma exploração robusta e eficiente das distribuições posteriores, permitindo não apenas a estimação dos parâmetros constitutivos, mas também a quantificação das incertezas associadas a esses parâmetros e a comparação probabilística entre modelos concorrentes por meio da evidência Bayesiana. Os resultados evidenciam a importância do uso de métodos que incorporam explicitamente as incertezas experimentais e inferenciais, uma vez que diferentes modelos podem apresentar ajustes semelhantes sob uma análise exclusivamente determinística.

**Palavras-chave**

Materiais hiperelásticos • Modelo de energia de deformação • Problema inverso • Transitional Markov Chain Monte Carlo (TMCMC)

# 1 Introduction

In recent years, the mechanical behavior of soft biological tissues has been widely studied due to their importance in essential functions such as movement, body stabilization, and posture changes. Through this study, it is possible to understand diseases that alter the mechanical behavior of these tissues. One example is osteoarthritis, which alters the mechanical response of muscle tissues due to repetitive loading [1]. Another example is the compression characterization of cerebral white matter under varying strain rates [2]. Additionally, it allows understanding the high compressions experienced by muscle tissues during car accidents or contact sports practice, such as boxing [3]. This understanding contributes to a better comprehension of changes in the mechanical behavior of muscle tissues, enabling diagnosis at early stages of disease [4].

Due to the difficulty in obtaining biological samples for ethical and bureaucratic reasons, as well as the complexity of testing these samples, which are moist and sensitive, the experimental results usually present large discrepancies [5]. An additional source of variability lies in the nature of the material itself, in a synthetic material, the mechanical properties of each component are individually known, unlike biological tissues, in which the individual mechanical properties are unknown and difficult to determine. In view of these challenges, the use of synthetic materials to simulate the mechanical behavior of soft biological tissues becomes attractive. Studies such as those by Moreira and Nunes [6] and Ruiz et al.[7] have adopted a similar approach.

The study of the mechanical behavior of soft biological tissues can be done using hyperelasticity theory, so the constitutive equation requires the definition of a scalar function known as strain energy. However, there is no strain energy model that universally represents these materials [8]. Consequently, many researchers continue to develop models that can represent this class of materials more satisfactorily. Examples of such models include the Mooney-Rivlin model [9], Merodio and Ogden [10], Lopez-Pamies [11], Anssari-Benam [12] and Stumpf [13]. Thus, obtaining experimental data plays a fundamental role in the development and improvement of these models.

Considering that soft biological tissues are described in the literature according to hyperelasticity theory, and taking into account the intrinsic characteristics of these tissues, such as the presence of fibers inside them, which characterizes anisotropic behavior, several studies such as that by Moreira and Nunes [6] have simulated their mechanical behavior through a hyperelastic matrix reinforced by a family of parallel fibers. This approach defines the material as transversely isotropic hyperelastic.

In this context, the present work aims to apply a model class selection technique to experimental results from compression tests on a silicone rubber and on a composite with the same rubber (matrix) and unidirectional cotton fibers (reinforcement). The idea is to determine which model best fits the experimental data using a Bayesian approach. Inverse problem techniques are employed to estimate the material parameters while explicitly accounting for their associated uncertainties, rather than providing only point estimates [14]. This probabilistic framework allows quantifying the confidence in the identified parameters, which is particularly important for materials with high variability and experimental dispersion. Moreover, the Transitional Markov Chain Monte Carlo (TMCMC) method is adopted due to its robustness and efficiency, and because it provides, as a byproduct, an estimate of the model evidence [15, 16]. This feature enables the quantitative comparison of competing strain energy models and the selection of the model that most plausibly describes the experimental data.

# 2 Methodology

## 2.1 Experimental Procedure

Five prismatic specimens (CP) of vulcanized silicone and five of a composite with the same silicone rubber and unidirectional cotton fibers were manufactured. For their fabrication, an aluminum mold with internal dimensions

of 128.50 mm length, 12.50 mm width, and 25.70 mm thickness was used, with a glass plate as a base. A layer of TecGlaze-N carnauba mold release wax was applied on the glass and inside the mold. Then, a cyanoacrylate-based adhesive was used to fix the mold to the glass.

The fabrication of pure silicone specimens consisted of mixing Moldflex 4-150 RTV silicone rubber and Moldflex catalyst in a beaker at an approximate ratio of 187(A):1(B). Then, the mixture was poured into the mold. The mold with the glass base and the liquid silicone inside can be seen in Fig. 1. After 72 hours, the time required for curing, the sample was demolded and cut into specimen dimensions (27.14 mm x 12.06 mm x 26.74 mm), considering the average of the five fabricated specimens. These dimensions were chosen to ensure the same height and cross-sectional area recommended by ISO 7743:2017 [17].

Figure 1: Mold used for specimen fabrication.

For the fabrication of composites with horizontally oriented cotton fibers (Fig. 2), the same Moldflex 4-150 RTV silicone rubber and Moldflex catalyst were mixed in a beaker, following the previously described ratio. However, for composite fabrication, the procedure was repeated several times to completely fill the mold, since the pot life of the mixture is short, making it difficult to pour due to high viscosity. Then, a layer of silicone rubber was placed inside the mold, followed by a strip of cotton, and to maintain the pattern, each layer was weighed on a scale. At the end of the process, the ten stacked cotton fibers corresponded to approximately 11% of the specimen volume fraction. The cutting process and final sample dimensions followed the same procedure described for pure silicone.

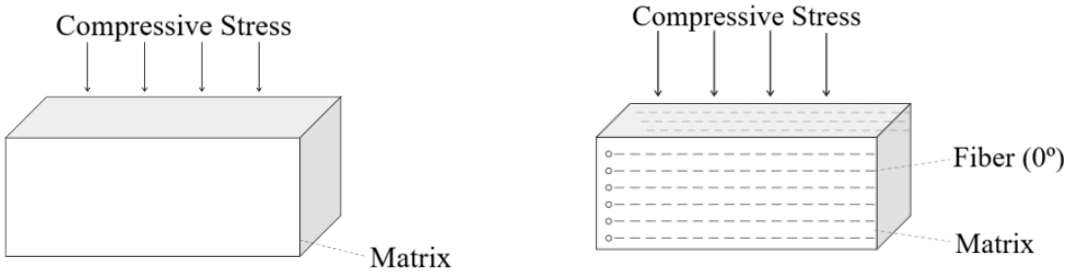


(a) Pure silicone.

(b) Composite.

Figure 2: Schematic drawings of the samples.

Compression tests were conducted using a universal testing machine from *Shimadzu* (model *AG-X plus*, Japan). To measure the applied force during each test stage, a 100 kN load cell coupled to the machine was used.

Displacement fields were determined using the Digital Image Correlation (DIC) method. DIC is a numerical optical method that uses a high-resolution camera to capture images of the sample before and after mechanical loading [6]. This method presents advantages compared to traditional methods such as strain gauges, since no contact with the tested sample is required. Moreover, in the study of materials with anisotropic properties, DIC stands out as a remarkable tool because it allows a global analysis of displacement fields. For image acquisition, a high-resolution CCD camera *(Charge Coupled Device)* from *Flir* (model *BFS-U3-32S4M-C Blackfly*, USA) with a 13–130 mm lens and an LED light source were used to homogenize illumination and reduce external influences. The experimental setup is shown in Fig. 3.

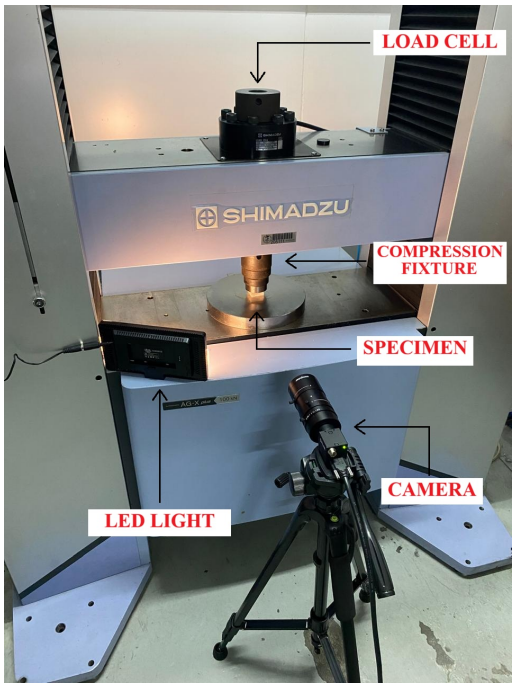


Figure 3: Experimental setup used in the compression tests.

The camera remained at a fixed distance from the sample during all tests, so that the pixel-to-millimeter ratio remained constant for all captured images. The camera focus was adjusted to the central region of the sample, which was the region of interest. Before each test, a layer of LUB lubricant (Tek Bond brand) was applied to the top of the sample and the machine base, allowing the specimen to slide during compression. The tests were performed at a speed of 10 mm/min, as specified by ISO 7743:2017. Additionally, the camera was configured to capture images every 0.5 seconds. It is important to highlight that all tests were conducted in a laboratory at approximately 23 ºC.

After the tests, the images were stored for later processing in a digital image correlation program, such as the open-source Python software developed by Deus Filho et al. [18]. Displacement fields were obtained for all tested samples, and stretches were calculated from them.

## 2.2 Constitutive Equation for Hyperelastic Material

The constitutive equation for incompressible transversely isotropic hyperelastic materials is described by [19]:

$$\mathbf{T} = -p\mathbf{I} + 2\left[\frac{\partial W}{\partial I_1}\mathbf{B} - \frac{\partial W}{\partial I_2}\mathbf{B}^{-1} + \frac{\partial W}{\partial I_4}\mathbf{a}\otimes\mathbf{a} + \frac{\partial W}{\partial I_5}(\mathbf{a}\otimes\mathbf{B}\mathbf{a} + \mathbf{B}\mathbf{a}\otimes\mathbf{a})\right] \tag{1}$$

where $\mathbf{T}$ is the Cauchy stress, $\mathbf{B}$ is the Cauchy-Green deformation tensor, $\mathbf{I}$ is the identity matrix, $p$ is a hydrostatic pressure related to the incompressibility assumption, $\mathbf{a}$ indicates the fiber orientation, and $W$ is the strain energy.

The principal invariants of the Cauchy-Green deformation tensor are measures that can be applied in representing the stress state in isotropic materials, and are defined as:

$$I_1 = \operatorname{tr}\mathbf{B} = \lambda_1^2 + \lambda_2^2 + \lambda_3^2 \tag{2}$$

$$I_2 = \frac{1}{2}\left[(\text{tr}\,\mathbf{B})^2 - \text{tr}(\mathbf{B}^2)\right] = \lambda_1^2\lambda_2^2 + \lambda_1^2\lambda_3^2 + \lambda_2^2\lambda_3^2 \tag{3}$$

$$I_3 = \det(\mathbf{B}) = \lambda_1^2\lambda_2^2\lambda_3^2 \tag{4}$$

where $\lambda$ represents the stretch, defined as the ratio between the current length of the specimen and its initial length.

Considering the incompressible material, the third invariant is assumed to be unity [10]. Therefore, the term related to $I_3$ does not appear in Eq. (1).

Due to the presence of fibers inside the material, the pseudo-invariants $I_4$ and $I_5$ arise, which are associated with anisotropic behavior. $I_4$ represents the influence of fiber stretch as the material is deformed, while $I_5$ is related to fiber stretch and shear [6],[20]. Thus:

$$I_4 = \mathbf{a}\cdot\mathbf{a} = \lambda_1^2\cos^2\alpha + \lambda_2^2\sin^2\alpha \tag{5}$$

$$I_5 = \mathbf{F}^T\mathbf{a}\cdot\mathbf{F}^T\mathbf{a} = \lambda_1^4\cos^2\alpha + \lambda_2^2\sin^2\alpha \tag{6}$$

where $\alpha$ represents the preferred fiber direction angle.

## 2.3 Strain Energy Models

Several strain energy models available in the literature are capable of representing the mechanical behavior of hyperelastic materials. Some are composed of invariants $I_1$ and $I_2$, which represent the matrix contribution (isotropic part), while others are composed of invariants $I_4$ and $I_5$, which represent the presence of a fiber family inside the composite (anisotropic part).

In the present work, six strain energy models were evaluated, three for isotropic hyperelastic materials and three for transversely isotropic hyperelastic materials.

The Mooney-Rivlin model [9] was formulated as a linear combination of the first two invariants of the Cauchy-Green deformation tensor

$$W = c_1(I_1 - 3) + c_2(I_2 - 3) \tag{7}$$

where $c_1$ and $c_2$ are material constants determined according to experimental results.

The Lopez-Pamies model [11] aims to be simple but capable of accurately predicting the mechanical behavior of rubber-like elastic solids

$$W = \frac{3^{1-\kappa}}{2\kappa}\mu(I_1^\kappa - 3^\kappa) \tag{8}$$

where $\kappa$ is a material parameter that must be greater than 0.5, and $\mu$ is the shear modulus and must be greater than 0.

The Anssari-Benam model [12], according to the author, aims to be more comprehensive

$$W = \frac{3(n-1)}{2n}\nu N\left[\frac{1}{3N(n-1)}(I_1 - 3) - \ln\left(\frac{I_1 - 3N}{3 - 3N}\right)\right] \tag{9}$$

where $n, N$ and $\nu$ are material parameters to be defined.

The Alastrué model [21] was proposed to representation soft biological tissues considering both isotropic and anisotropic contributions. It is important to highlight that, in the model formulation, invariant $I_6$ is associated with fiber stretch in two preferred directions; thus, only the terms related to invariants $I_1$ and $I_4$ are considered here

$$W = D_1[I_1 - 3] + D_2[\sqrt{I_4} - 1]^2 \tag{10}$$

where $D_1$ and $D_2$ are positive constants with units of MPa.

The Feng model [22] was developed to represent a transversely isotropic hyperelastic material

$$W = \frac{\mu}{2}[(I_1 - 3) + \zeta(I_4 - 1)^2 + \varphi(I_5 - I_4^2)] \tag{11}$$

where $\mu$ is the shear modulus and $\zeta, \varphi$ are dimensionless parameters.

Finally, Bonet-Burton model [23] was also proposed with the aim of representing a strain energy for transversely isotropic hyperelastic materials

$$W = [\beta + \gamma(I_4 - 1)](I_4 - 1) - \frac{\beta}{2}(I_5 - 1) \tag{12}$$

where $\beta$ and $\gamma$ are material constants with units of MPa.

Table 1: Isotropic and transversely isotropic strain energy models.

| Category | Model (Author) | Strain Energy ($W$) | Parameters |
|---|---|---|---|
| **Isotropic** | Mooney-Rivlin | $W = c_1(I_1 - 3) + c_2(I_2 - 3)$ | $c_1, c_2$ |
| | Lopez-Pamies | $W = \frac{3^{1-\kappa}}{2\kappa}\mu(I_1^\kappa - 3^\kappa)$ | $\kappa, \mu$ |
| | Anssari-Benam | $W = \frac{3(n-1)}{2n}\nu N\left[\frac{1}{3N(n-1)}(I_1 - 3) - \ln\left(\frac{I_1-3N}{3-3N}\right)\right]$ | $n, N, \nu$ |
| **Transversely Isotropic** | Alastrué et al. | $W = D_1[I_1 - 3] + D_2[\sqrt{I_4} - 1]^2$ | $D_1, D_2$ |
| | Feng et al. | $W = \frac{\mu}{2}[(I_1 - 3) + \zeta(I_4 - 1)^2 + \varphi(I_5 - I_4^2)]$ | $\mu, \zeta, \varphi$ |
| | Bonet-Burton | $W = [\beta + \gamma(I_4 - 1)](I_4 - 1) - \frac{\beta}{2}(I_5 - 1)$ | $\beta, \gamma$ |

## 2.4 Inverse Problem

In this work, the Transitional Markov Chain Monte Carlo (TMCMC) algorithm is employed for parameter estimation and model class selection. The objective is to identify which strain energy model best represents the experimental data obtained from compression tests [16]. The main advantages of this method arise from its Bayesian framework, using Bayes' Theorem, allowing the incorporation of prior information about the parameters $\mathbf{P}$ through the prior distribution $\pi(\mathbf{P})$ [16]. In a Bayesian approach, the method does not provide a single point estimate but rather a region where the parameters of interest may be located. This region indicates the probability associated with each point within it, highlighting the most probable points based on the posterior distribution $\pi(\mathbf{P}|\mathbf{Y})$ [14].

$$\pi(\mathbf{P}|\mathbf{Y}) = \frac{\pi(\mathbf{P})\pi(\mathbf{Y}|\mathbf{P})}{\pi(\mathbf{Y})} \tag{13}$$

Bayes' Theorem is described in Eq. (13) where $\mathbf{P}$ is the vector containing the uncertain model parameters and $\mathbf{Y}$ is the vector of observed experimental data used in the inversion process (stretch measurements in the compression test). The TMCMC, proposed by Ching & Chen [16], aims to avoid direct sampling of the posterior distribution. Initially, independent samples are drawn from a prior distribution. In subsequent steps, the sample distribution is gradually transformed to approach the posterior distribution. Thus, Bayes' Theorem is modified as follows:

$$\pi_j(\mathbf{P}|\mathbf{Y}) \propto \pi(\mathbf{P})\pi(\mathbf{Y}|\mathbf{P})^{p_j} \qquad j = 0, 1, ..., m \qquad 0 = p_0 < p_1 < ... < p_m = 1 \tag{14}$$

where the index $j$ denotes the stage number. It is easy to note that $\pi_0(\mathbf{P}|\mathbf{Y})$ is the prior distribution and $\pi_m(\mathbf{P}|\mathbf{Y})$ is the posterior distribution itself. The steps of the TMCMC algorithm are described below [24]:

1. Obtain $S$ samples $\mathbf{P}_{0,1}, \mathbf{P}_{0,2}, ..., \mathbf{P}_{0,S}$ from the prior distribution $\pi(\mathbf{P})$ using Monte Carlo simulation. Set $p_0 = 0$ and repeat steps 2 and 3 for $j = 0, 1, 2, ....$
2. Compute the likelihood distributions $\pi(\mathbf{Y}|\mathbf{P}_{j,k})$ and calculate the importance weights $w_{j,k} = \pi(\mathbf{Y}|\mathbf{P}_{j,k})^{p_{j+1}-p_j}$ for $k = \{1, 2, ..., S\}$. Note that $p_{j+1}$ should be chosen such that the COV of the importance weights is equal to 100%. Also compute the normalized weights $\bar{w}_{j,k}$.
3. According to the normalized weights $\bar{w}_{j,k}$, randomly select candidates from $\{\mathbf{P}_{j,1}, \mathbf{P}_{j,2}, ..., \mathbf{P}_{j,S}\}$, propose a new candidate according to the distribution $N\left(\mathbf{P}_{j,k}, \Sigma_j\right)$, and form the sequence $\mathbf{P}_{j+1,k}$, again for $k = \{1, 2, ..., S\}$.

$$\Sigma_j = \delta^2 \sum_{k=1}^{S} \bar{w}_{j,k}\left(\mathbf{P}_{j,k} - \sum_{n=1}^{S} \bar{w}_{j,n}\mathbf{P}_{j,n}\right) \cdot \left(\mathbf{P}_{j,k} - \sum_{n=1}^{S} \bar{w}_{j,n}\mathbf{P}_{j,n}\right)^T \tag{15}$$

The covariance matrix $\Sigma_j$ is described by Eq. (15), where $\delta$ is a tempering parameter. As a byproduct, the method can estimate the model evidence through the importance weights calculated during the execution of the algorithm [16].

$$\pi(Y|\mathcal{M}) \approx \prod_{j=0}^{m-1}\left(\frac{1}{S}\sum_{k=1}^{S} w_{j,k}\right) \tag{16}$$

$$\pi(\mathcal{M}_i|\mathbf{Y}) = \frac{\pi(\mathbf{Y}|\mathcal{M}_i)\pi(\mathcal{M}_i)}{\sum_{j=1}^{N_m} \pi(\mathbf{Y}|\mathcal{M}_j)\pi(\mathcal{M}_j)} \tag{17}$$

According to Ching & Wang [24], the model evidence for any model $\mathcal{M}$ can be approximated using Eq. (16). When evaluating more than one model, the probability of each model is given by Eq. (17), where the index $i$ denotes the model of interest and $N_m$ is the total number of evaluated models.

# 3 Results and Discussion

This section presents the results of parameter estimation and model class selection for two different material configurations subjected to compression. In Case 1, the mechanical response of a pure silicone specimen is described using three constitutive models formulated for isotropic materials. In Case 2, the material consists of a silicone rubber composite reinforced by horizontally oriented cotton fibers, thus requiring constitutive formulations capable of representing anisotropic effects. In both cases, model class selection is carried out within a Bayesian framework using the TMCMC algorithm, which enables the identification of the model that provides the most plausible description of the experimental data while accounting for both data fit and model complexity.

## 3.1 Case 1: Pure Silicone

Figure 4 shows the compression stress–stretch curves obtained for the pure silicone specimens, together with the corresponding mean response and standard deviation bars. The experimental curves revealing the expected nonlinear mechanical behavior of the material.

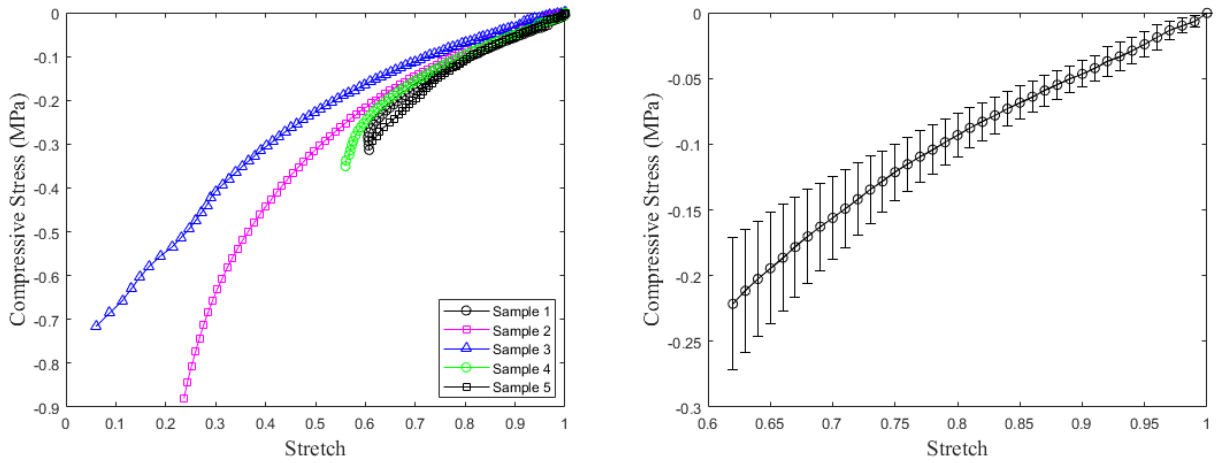


(a) Compression stress–stretch curves.

(b) Mean curve with error bars.

Figure 4: Compression stress–stretch curves of the tested samples.

The experimental data employed in the inverse analysis correspond to the mean curve shown in Fig. 4b, to which Gaussian noise with zero mean and standard deviation equal to 0.005 MPa was added in order to represent measurement uncertainty. Table 2 summarizes the constitutive models considered in this case, as well as the corresponding vectors of uncertain parameters to be estimated through the Bayesian inverse problem.

Within the TMCMC framework, a higher posterior probability indicates a model that achieves a more plausible balance between quality of fit and model complexity. Therefore, when two competing models provide similar agreement with the experimental data, the Bayesian evidence naturally favors the more parsimonious formulation, that is, the one requiring less information to explain the observations [15].

The estimated parameters for the three isotropic models are listed in Table 3. In general, the coefficients of variation $\sigma/\eta$ (where $\sigma$ and $\eta$ denote the standard deviation and the mean of the posterior distribution of the parameter, respectively) are low, indicating relatively concentrated posterior distributions and, consequently, stable parameter estimates. The only exception is the Ansari-Benam model, whose higher relative dispersion suggests greater difficulty in simultaneously identifying all three uncertain parameters.

Table 2: Models considered for Case 1.

| **Model** | **Equation** | **Vector of Uncertain Parameters** |
|---|---|---|
| Mooney-Rivlin | Eq. (7) | $\mathbf{P} = \{c_1, c_2\}^T$ |
| Lopez-Pamies | Eq. (8) | $\mathbf{P} = \{\kappa, \mu\}^T$ |
| Ansari-Benam | Eq. (9) | $\mathbf{P} = \{n, N, \mu\}^T$ |

Table 3: Estimation of uncertain parameters for the different considered models.

| **Model** | **Parameter** | **Mean** | $\frac{\sigma}{\eta}$ **(%)** |
|---|---|---|---|
| Mooney-Rivlin | $c_1$ | 0.04237 | 0.13 |
| | $c_2$ | 0.02849 | 0.13 |
| Lopez-Pamies | $\kappa$ | 4.43545 | 0.11 |
| | $\mu$ | 0.14918 | 0.02 |
| Ansari-Benam | $n$ | 32.69826 | 8.1 |
| | $N$ | 18.43741 | 13.18 |
| | $\nu$ | 0.13960 | 5.7 |

Figures 5 and 6 present the model predictions obtained using the posterior mean values of the estimated parameters, together with the corresponding credible intervals. All three models reproduce the experimental trend reasonably well over the analyzed stretch range, which indicates that, within this restricted domain, distinct constitutive formulations may lead to similar macroscopic responses.

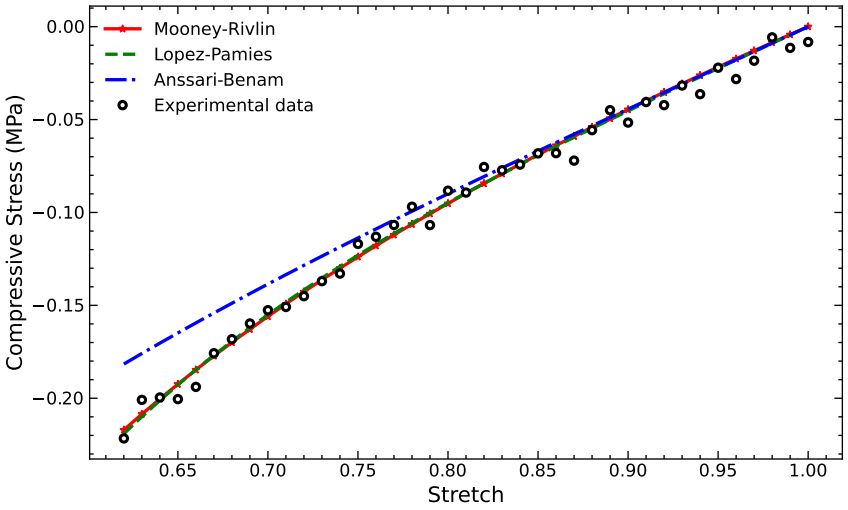


Figure 5: Model predictions using the posterior mean estimates for Case 1.

Although all models provide satisfactory fits, some relevant differences emerge from the uncertainty analysis. The Ansari-Benam model shows the poorest overall performance, which may indicate practical identifiability issues associated with the simultaneous estimation of its three parameters. Such behavior may be related to parameter correlation, low sensitivity of the response with respect to some parameters, or partial redundancy in their roles within the constitutive formulation. A more detailed sensitivity and identifiability analysis will be conducted in future work.

The relatively small differences among the fitted curves are likely associated with the limited stretch range considered in the present analysis. In such a situation, parameter estimation alone is not sufficient to discriminate between competing constitutive models, which reinforces the importance of Bayesian model class selection. In particular, the

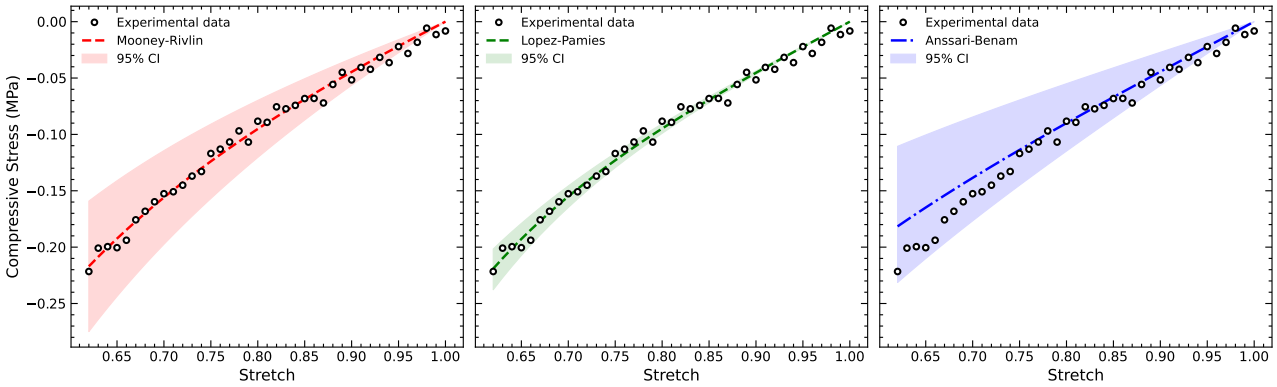


Figure 6: Model predictions and credible intervals for Case 1.

Mooney-Rivlin model exhibits a wider credible interval than the Lopez-Pamies model, suggesting a higher level of uncertainty in the inferred parameters and, consequently, a less informative posterior distribution.

The model class selection results are summarized in Table 4. In addition to the logarithm of the evidence, the table includes the logarithm of the posterior mean likelihood, which reflects the quality of fit to the data, and the information gain term, which measures the amount of information extracted from the data and acts as a penalty against unnecessarily complex or weakly identifiable models.

Table 4: Model class selection for Case 1.

| **Model** | **Data Fitting** | **Information Gain** | **ln**(evidence) | **Probability (%)** |
|---|---|---|---|---|
| Mooney-Rivlin | −26.17 | 11.95 | −38.12 | 30.36 |
| Lopez-Pamies | **−25.47** | **11.82** | **−37.29** | **69.63** |
| Ansari-Benam | −47.93 | 11.25 | −59.18 | 0 |

Table 4 confirms that the Mooney-Rivlin and Lopez-Pamies models provide comparable fits to the data, whereas the Ansari-Benam model is clearly less competitive. However, the Lopez-Pamies model achieves the best compromise between data agreement and model plausibility, resulting in the highest evidence and posterior probability. This result indicates that the Lopez-Pamies formulation is the most plausible constitutive description for the compression response of the pure silicone specimen within the analyzed experimental range.

Finally, Fig. 7 shows the posterior distributions of the parameters associated with the selected model, namely the Lopez-Pamies model. The relatively concentrated marginals are consistent with the low coefficients of variation reported in Table 3, supporting the robustness of the inferred parameter values.

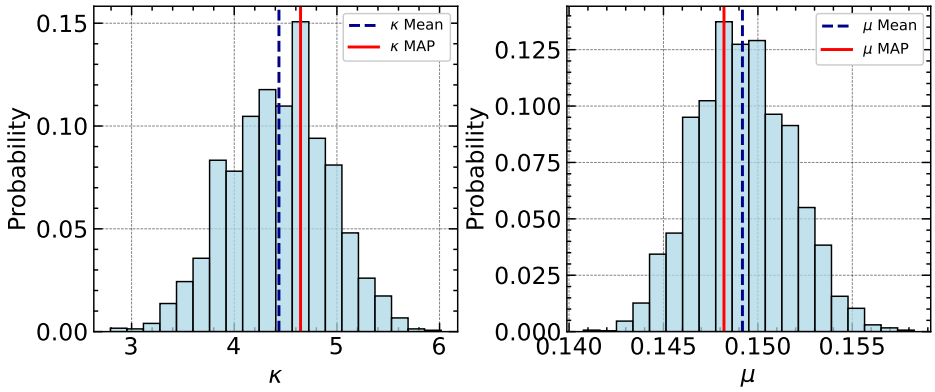


Figure 7: Posterior distributions of the parameters for the Lopez-Pamies model.

## 3.2 Case 2: Composite

This subsection presents the results of parameter estimation and model class selection for the fiber-reinforced composite specimen. In contrast to Case 1, the presence of horizontally oriented cotton fibers introduces anisotropic effects into the mechanical response, so that purely isotropic constitutive laws are no longer sufficient to properly describe the observed behavior. For this reason, anisotropic strain energy density models were considered for the composite response.

Additionally, the Bonet and Burton model considered describes only the anisotropic contribution of the material, making it necessary to combine it with another model capable of properly representing the isotropic part. Based on the results presented above, the isotropic model that showed the best performance was the Lopez-Pamies model. Therefore, it will be adopted to represent the isotropic contribution of the material.

Figure 8 presents the compression stress–stretch curves obtained for the composite samples, together with the corresponding mean response and standard deviation bars. As in the previous case, the experimental curves exhibit the expected nonlinear mechanical behavior of the material, and the observed dispersion remains within an acceptable range for this type of test.

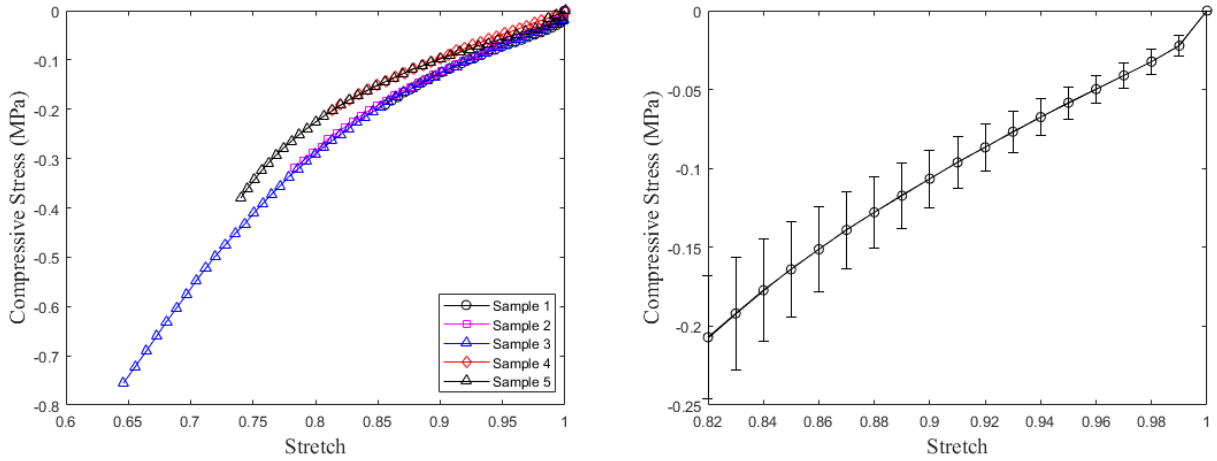


(a) Compression stress–stretch curves.

(b) Mean curve with error bars.

Figure 8: Compression stress–stretch curves of the tested composite samples.

Table 5 summarizes the constitutive models considered for the composite case and their corresponding vectors of uncertain parameters. The posterior estimates obtained for each model are reported in Table 6.

Table 5: Models considered for Case 2.

| **Model** | **Equation** | **Vector of Uncertain Parameters** |
|---|---|---|
| Alastrue et al. | Eq. (10) | $\mathbf{P} = \{D_1, D_2\}^T$ |
| Feng et al. | Eq. (11) | $\mathbf{P} = \{\mu, \xi, \varphi\}^T$ |
| Bonet-Burton | Eq. (12) | $\mathbf{P} = \{\beta, \gamma\}^T$ |

*Estimated parameters by the Lopez-Pamies model.

Figures 9 and 10 compare the predictions of the three models against the experimental data. It can be observed that all formulations are able to reproduce the overall trend of the composite response with good accuracy, leading to very similar fitted curves over the analyzed stretch range. This result indicates that, from the perspective of data fitting alone, the three constitutive models provide a comparable description of the experimental response.

Despite the close agreement in terms of the fitted mean response, the uncertainty associated with each model is not the same. In particular, the models proposed by Alastrue et al. and Feng et al. exhibit broader credible intervals, indicating greater uncertainty in the inferred parameters and, consequently, a less concentrated posterior

Table 6: Estimation of uncertain parameters for the different considered models for Case 2.

| **Model** | **Parameter** | **Mean** | $\frac{\sigma}{\eta}$ **(%)** |
|---|---|---|---|
| Alastrue et al. | $D_1$ | 0.18206 | 0.20 |
| | $D_2$ | 0.00835 | 2.58 |
| Feng et al. | $\mu$ | 0.05822 | 0.80 |
| | $\xi$ | -0.96158 | 8.34 |
| | $\varphi$ | 0.34341 | 0.12 |
| Bonet-Burton | $\kappa^*$ | 4.43545 | 0.11 |
| | $\mu^*$ | 0.14918 | 0.02 |
| | $\beta$ | 0.00338 | 0.20 |
| | $\gamma$ | 0.09674 | 0.27 |

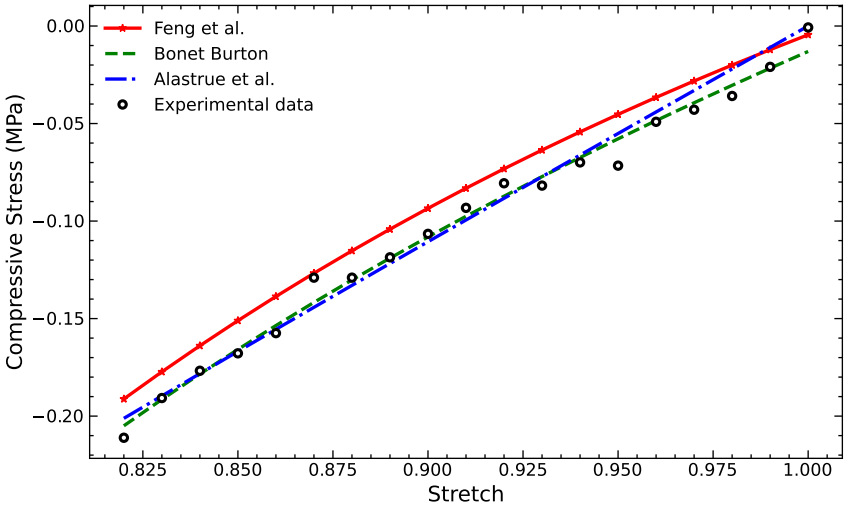


Figure 9: Model predictions using the posterior mean estimates for Case 2.

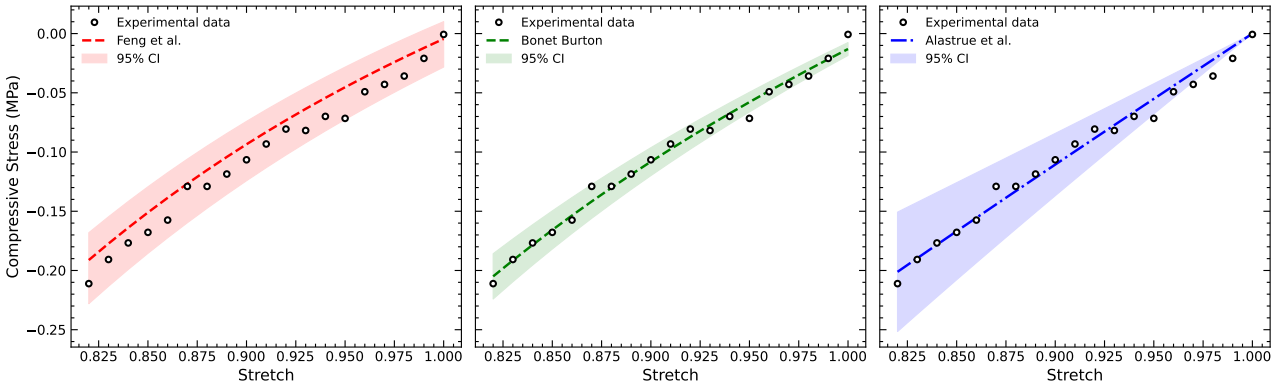


Figure 10: Model predictions and credible intervals for Case 2.

description. By contrast, the Bonet–Burton model leads to a more stable inverse solution, with narrower uncertainty bounds and a more informative posterior distribution.

The model class selection results are summarized in Table 7. In this case, the Bonet–Burton model is identified as the most plausible constitutive representation for the composite material, with a posterior probability of 93.63%. Although the three models provide similar fits to the experimental data, the Bonet–Burton formulation yields the

best compromise between fitting quality and uncertainty quantification, resulting in the most favorable evidence value.

Table 7: Model class selection for Case 2.

| **Model** | **Data Fitting** | **Information Gain** | **ln**(evidence) | **Probability (%)** |
|---|---|---|---|---|
| Feng et al. | −31.18 | 10.35 | −41.53 | 0.07 |
| Bonet-Burton | **−24.90** | **9.15** | **−34.05** | **93.63** |
| Alastrue et al. | −23.87 | 12.88 | −36.75 | 6.30 |

This result is also physically meaningful. In the Bonet–Burton formulation, the isotropic contribution is represented through a structure consistent with the Lopez–Pamies model, which was previously identified in Case 1 as the most plausible constitutive model for the pure silicone matrix. Therefore, the superior performance of the Bonet–Burton model in the composite case is coherent with the results obtained for the homogeneous material, since it combines an isotropic contribution already shown to be appropriate for the matrix with an additional term capable of accounting for the anisotropic effects introduced by the fiber reinforcement.

From a Bayesian perspective, this interpretation is further supported by the information gain values. Since the three models achieve relatively close fits, the final model selection is strongly influenced by the uncertainty associated with parameter inference. The larger uncertainty observed in the Alastrue et al. and Feng et al. models leads to a less favorable balance between posterior concentration and explanatory capability. As a result, the Bonet–Burton model presents the lowest information gain among the competing formulations and is therefore selected as the most plausible model for describing the compression response of the fiber-reinforced composite.

Accordingly, Fig. 11 shows the posterior distributions of the inferred parameters for the selected model, namely the Bonet–Burton model. These distributions provide additional insight into the uncertainty associated with the estimated parameters and reinforce the robustness of the model selection result.

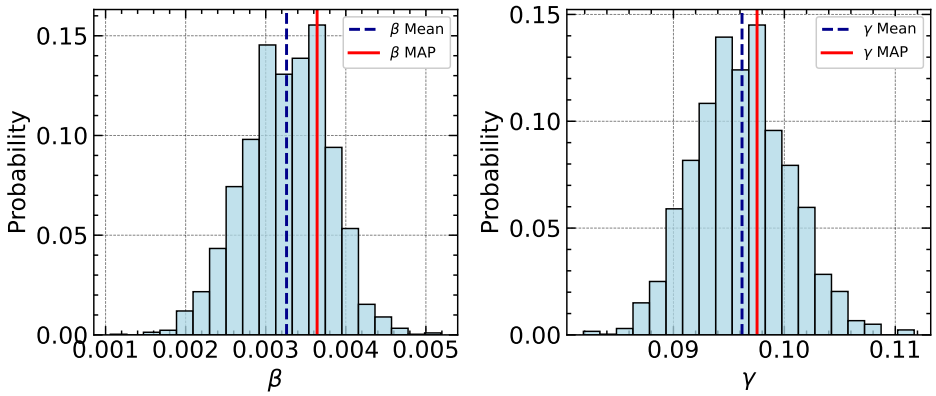


Figure 11: Posterior distributions of the parameters for the Bonet–Burton model.

# 4 Conclusion

In this work, the TMCMC framework proved to be an effective tool for both parameter estimation and Bayesian model class selection in the constitutive modeling of materials subjected to compression. In addition to providing posterior estimates for the uncertain parameters, the method enabled a consistent comparison among competing strain energy density functions by simultaneously accounting for quality of fit, parameter uncertainty, and model plausibility.

For the homogeneous material, the Lopez–Pamies model was identified as the most plausible constitutive description among the isotropic formulations considered. Although the Mooney–Rivlin and Lopez–Pamies models provided similarly good agreement with the experimental data, the latter achieved the best balance between fit quality and uncertainty, resulting in the highest model evidence. The corresponding posterior distributions and narrower credible intervals further indicate greater robustness and confidence in the inferred parameters.

For the composite material reinforced by horizontally oriented cotton fibers, the Bayesian model class selection identified the Bonet–Burton model as the most plausible among the anisotropic formulations considered. Although

the competing models yielded very similar fits to the experimental data, the uncertainty associated with the Alastrue et al. and Feng et al. models was larger, leading to a less favorable balance between predictive capability and posterior concentration. As a result, the Bonet–Burton model presented the most favorable evidence and was selected as the most plausible constitutive representation for the composite response.

This result is also physically consistent with the findings obtained for the pure silicone case. Since the isotropic contribution of the Bonet–Burton formulation is based on the Lopez–Pamies model, its selection for the composite material is coherent with the previous identification of Lopez–Pamies as the most suitable model for the silicone matrix. In this sense, the Bonet–Burton formulation provides a constitutive description that combines an appropriate representation of the isotropic matrix behavior with an additional contribution capable of capturing the anisotropic effects introduced by the cotton fiber reinforcement.

Overall, the results demonstrate the potential of TMCMC as a robust and comprehensive framework for constitutive parameter identification and model discrimination. By combining uncertainty quantification, posterior inference, and evidence-based model comparison, the proposed approach provides a reliable basis for selecting constitutive models capable of representing the mechanical behavior of both isotropic and anisotropic hyperelastic materials. Future investigations may extend this analysis by incorporating additional loading conditions, broader deformation ranges, and sensitivity or identifiability studies in order to further assess the predictive capabilities and physical interpretability of the competing models.

## Acknowledgments

This study was financed in part by the Coordenação de Aperfeiçoamento de Pessoal de Nível Superior - Brasil (CAPES) - Finance Code 001. The authors would like also to thank the other sponsoring agencies, CNPq - Conselho Nacional de Desenvolvimento Científico e Tecnológico and FAPERJ - Fundação Carlos Chagas Filho de Amparo à Pesquisa do Estado do Rio de Janeiro.

## References

[1] D. Correa and S. A. Lietman, "Articular cartilage repair: Current needs, methods and research directions," *Seminars in Cell & Developmental Biology*, vol. 62, p. 67–77, 2017. Available at: https://doi.org/10.1016/j.semcdb.2016.07.013

[2] S. Cheng and L. E. Bilston, "Unconfined compression of white matter," *Journal of Biomechanics*, vol. 40, no. 1, p. 117–124, 2007. Available at: https://doi.org/10.1016/j.jbiomech.2005.11.004

[3] T. Siebert, O. Till, and R. Blickhan, "Work partitioning of transversally loaded muscle: experimentation and simulation," *Computer Methods in Biomechanics and Biomedical Engineering*, vol. 17, no. 3, p. 217–229, 2012. Available at: https://doi.org/10.1080/10255842.2012.675056

[4] A. Ansardamavandi, M. Tafazzoli-Shadpour, R. Omidvar, and I. Jahanzad, "Quantification of effects of cancer on elastic properties of breast tissue by atomic force microscopy," *Journal of the Mechanical Behavior of Biomedical Materials*, vol. 60, p. 234–242, 2016. Available at: https://doi.org/10.1016/j.jmbbm.2015.12.028

[5] A. Leibinger, A. E. Forte, Z. Tan, M. J. Oldfield, F. Beyrau, D. Dini, and F. Rodriguez y Baena, "Soft tissue phantoms for realistic needle insertion: A comparative study," in *Annals of Biomedical Engineering*, vol. 44, no. 8, 2015, p. 2442–2452. Available at: https://doi.org/10.1007/s10439-015-1523-0

[6] C. S. Moreira and L. C. S. Nunes, "Effects of fiber orientation in a soft unidirectional fiber-reinforced material under simple shear deformation," *International Journal of Non-Linear Mechanics*, vol. 111, pp. 72–81, 2019. Available at: https://doi.org/10.1016/j.ijnonlinmec.2019.02.001

[7] O. Grimaldo Ruiz, M. Rodriguez Reinoso, E. Ingrassia, F. Vecchio, F. Maniero, V. Burgio, M. Civera, I. Bitan, G. Lacidogna, and C. Surace, "Design and mechanical characterization using digital image correlation of soft tissue-mimicking polymers," *Polymers*, vol. 14, no. 13, p. 2639, 2022. Available at: https://doi.org/10.3390/polym14132639

[8] M. Destrade, G. Saccomandi, and I. Sgura, "Methodical fitting for mathematical models of rubber-like materials," *Proceedings of the Royal Society A: Mathematical, Physical and Engineering Science*, vol. 473, no. 2198, p. 20160811, 2017. Available at: https://doi.org/10.1098/rspa.2016.0811

[9] R. S. Rivlin, "Large elastic deformations of isotropic materials IV. further developments of the general theory," *Philosophical Transactions of the Royal Society of London, Series A: Mathematical and Physical Sciences*, vol. 241, no. 835, pp. 379–397, 1948. Available at: https://doi.org/10.1098/rsta.1948.0024

[10] J. Merodio and R. W. Ogden, "Mechanical response of fiber-reinforced incompressible non-linearly elastic solids," *International Journal of Non-Linear Mechanics*, vol. 40, no. 2, pp. 213–227, 2005. Available at: https://doi.org/10.1016/j.ijnonlinmec.2004.05.003

[11] O. Lopez-Pamies, "A new I1-based hyperelastic model for rubber elastic materials," *Comptes Rendus Mécanique*, vol. 338, no. 1, pp. 3–11, 2010. Available at: https://doi.org/10.1016/j.crme.2009.12.007

[12] A. Anssari-Benam, "On a new class of non-gaussian molecular-based constitutive models with limiting chain extensibility for incompressible rubber-like materials," *Mathematics and Mechanics of Solids*, vol. 26, no. 11, pp. 1660–1674, 2021. Available at: https://doi.org/10.1177/10812865211001094

[13] F. Stumpf, "An accurate and efficient constitutive framework for finite strain viscoelasticity applied to anisotropic soft tissues," *Mechanics of Materials*, vol. 161, p. 104007, 2021. Available at: https://doi.org/10.1016/j.mechmat.2021.104007

[14] J. P. Kaipio and C. Fox, "The bayesian framework for inverse problems in heat transfer," *Heat Transfer Engineering*, vol. 32, no. 9, pp. 718–753, 2011. Available at: https://doi.org/10.1080/01457632.2011.525137

[15] W. Betz, I. Papaioannou, and D. Straub, "Transitional markov chain monte carlo: observations and improvements," *Journal of Engineering Mechanics*, vol. 142, no. 5, p. 04016016, 2016. Available at: https://doi.org/10.1061/(ASCE)EM.1943-7889.0001066

[16] J. Ching and Y.-C. Chen, "Transitional markov chain monte carlo method for bayesian model updating, model class selection, and model averaging," *Journal of Engineering Mechanics*, vol. 133, no. 7, pp. 816–832, 2007. Available at: https://doi.org/10.1061/(ASCE)0733-9399(2007)133:7(816)

[17] International Organization for Standardization, "Rubber, vulcanized or thermoplastic — determination of compression stress-strain properties," 2017, ISO 7743:2017. Available at: https://www.iso.org/standard/72784.html

[18] J. C. A. de Deus Filho, L. C. da Silva Nunes, and J. M. C. Xavier, "iCorrVision-2D: An integrated python-based open-source digital image correlation software for in-plane measurements (part 1)," *SoftwareX*, vol. 19, p. 101131, 2022. Available at: https://doi.org/10.1016/j.softx.2022.101131

[19] G. A. Holzapfel, "Nonlinear solid mechanics: A continuum approach for engineering." *John Wiley & Sons Ltd*, 2000.

[20] C. O. Horgan and J. G. Murphy, "Simple shearing of soft biological tissues," *Proceedings of the Royal Society A: Mathematical, Physical and Engineering Sciences*, vol. 467, no. 2127, pp. 760–777, 2010. Available at: https://doi.org/10.1098/rspa.2010.0288

[21] V. Alastrué, E. Peña, M. A. Martínez, and M. Doblaré, "Experimental study and constitutive modelling of the passive mechanical properties of the ovine infrarenal vena cava tissue," *Journal of Biomechanics*, vol. 41, no. 14, pp. 3038–3045, 2008. Available at: https://doi.org/10.1016/j.jbiomech.2008.07.008

[22] Y. Feng, R. J. Okamoto, R. Namani, G. M. Genin, and P. V. Bayly, "Measurements of mechanical anisotropy in brain tissue and implications for transversely isotropic material models of white matter," *Journal of the Mechanical Behavior of Biomedical Materials*, vol. 23, pp. 117–132, 2013. Available at: https://doi.org/10.1016/j.jmbbm.2013.04.007

[23] J. Bonet and A. J. Burton, "A simple orthotropic, transversely isotropic hyperelastic constitutive equation for large strain computations," *Computer Methods in Applied Mechanics and Engineering*, vol. 162, no. 1, pp. 151–164, 1998. Available at: https://doi.org/10.1016/S0045-7825(97)00339-3

[24] J. Ching and J.-S. Wang, "Application of the transitional markov chain monte carlo algorithm to probabilistic site characterization," *Engineering Geology*, vol. 203, pp. 151–167, 2016. Available at: https://doi.org/10.1016/j.enggeo.2015.10.015